LAWRENCE
LIVERMORE
NATIONAL
LABORATORY

LLNL-CONF-748304

# In-situ characterization of tungsten microcracking in Selective Laser Melting

B. Vrancken, W. E. King, M. J. Matthews

March 21, 2018

10th Conference on Photonic Technologies # LANE 2018
Furth, Germany
September 3, 2018 through September 6, 2018

## Disclaimer

Available online at www.sciencedirect.com

ScienceDirect

Procedia 00 (2018) 000–000

www.elsevier.com/locate/procedia

10th Conference on Photonic Technologies – LANE 2018

# In-situ characterization of tungsten microcracking in Selective Laser Melting

B. Vrancken[a,*], W.E. King[a], M.J. Matthews[a]

[a] *Lawrence Livermore National Laboratory, 7000 East Avenue, Livermore 94550 CA, USA*

* Corresponding author. Tel.: +1-925-423-0850. *E-mail address:* vrancken1@llnl.gov

**Abstract**

Additive Manufacturing is a promising way of processing tungsten, with opportunities to create more complex parts than are possible using other powder metallurgical routes. This may lead to extended applications such as collimators, in fusion reactors, or in other structurally loaded, high temperature environments. The poor thermal shock resistance and ductile-to-brittle transition that occurs in tungsten above room temperature are challenges that hinder production of fully dense and crack free parts. This research employs high speed in-situ monitoring of Selective Laser Melting of single tracks to visualize crack initiation and propagation. The circumstances that lead to cracking are correlated with microstructural morphology and processing conditions.



*Keywords:* Tungsten; Additive Manufacturing; Selective Laser Melting; Microcracking; In-situ monitoring; Laser powder bed fusion

## 1. Introduction

Because of its high melting point, low thermal expansion, high thermal conductivity, low neutron yield under energetic particle irradiation, low sensitivity to hydrogen, and other favorable properties, tungsten (W) is currently considered a top candidate as a plasma facing material in fusion reactors. In that environment, it would have to withstand steady state thermal loads of 5-20 MW/m², but also transient thermal loads of up to 10 MJ/m$^2$ [1]. This requires excellent thermal and mechanical properties at high temperatures that few materials can deliver. One of the disadvantages of tungsten is its low recrystallization temperature, which is the effective upper limit of its useful temperature operating range, as the mechanical properties deteriorate above it [1]. Of equal importance are the low temperature properties to avoid problems during start-up of the reactor. In this sense, the brittle nature of tungsten at low temperature and poor thermal shock resistance are the limiting factors [1].

Previous processing of tungsten and tungsten alloys via Selective Laser Melting (SLM) has resulted in densities up to 98% [2], [3], but microcracks were never avoided [2]–[5]. It is hypothesized that the residual stress in combination with the ductile-to-brittle transition, which lies anywhere between 200°C [6], [7] and 400°C [8]–[10] or even higher for higher impurity contents [11], is the cause of these cracks.

Several studies have investigated the effect of alloying on the thermal properties of tungsten, and three types of alloys stand out: (1) Potassium doped W incorporates nanosized potassium bubbles to pin the grain boundaries and dislocations, and thereby increase high temperature strength [12], (2) Rhenium solid solution strengthened W (W26Re in particular) in which the Re changes dislocation morphology and influences the behavior of interstitial atoms, leading to an increased low temperature ductility [13], and (3) Oxide-dispersion strengthened W in which $La_2O_3$, $Y_2O_3$, or another oxide affect the high temperature strength and ductile-to-brittle transition with varying amounts of success [9], [10], [14], [15].

For fusion applications, the new tungsten-based materials under investigation are typically subjected to thermal loads up to 1 GW/m$^2$ [1], [12], [16]. By comparison, and because SLM

consists of rapid *melting* and *solidification* rather than heating and cooling, the thermal loads experienced during SLM are one to two orders of magnitude higher than the transient thermal loads in fusion applications. The argument can be made that if the tungsten-based material can be produced by laser additive manufacturing without microcracking, it will also be able to withstand the steady state and transient thermal loads it would experience serving as a plasma-facing material.

A fundamental understanding of the formation of the microcracks during SLM of W is still lacking since existing literature has focused on a posteriori characterization of the microcrack network. For the first time, this work investigates the microcracking in SLM by using in-situ high-speed video to uncover the influence of process parameters on the crack formation.

**Nomenclature**

| | |
|---|---|
| $P$ | laser power [W] |
| $v$ | scan speed [mm/s] |
| λ | wavelength [nm] |
| SLM | Selective Laser Melting |

## 2. Materials & Methods

The high-speed imaging platform has been described previously in Ref. [17]. A Photron SA-X2 high speed camera was used to capture the high-speed videos. A 768x328 pixels frame size was used at a 50 kHz frame rate, which translated to a 620x265 µm field of view. The field of view was stationary, and the laser scanned across the image. The shutter rate was set to the minimum to eliminate melt pool irradiance. The experimental setup is shown in Figure 1. A dichroic filter that allowed all wavelengths above 1000 nm to pass was used to achieve top-down vision by reflecting the wavelengths used for imaging towards the camera. The optics consisted of a 10x microscope objective with co-axial illumination from a Cavilux HF 500 W low coherence laser source (λ = 808 nm) pulsed at 1 µs. Ar was flown freely over the base plate at a rate of 0.5 l/min. A 1070 nm wavelength JK FL600 Yb:glass fiber laser operating in continuous wave mode with a maximum power output of 600W and 50 µm $1/e^2$ beam diameter was used to scan single 2 mm long vectors on a tungsten plate. The 2 mm thick W plate was cut from a 25.4 mm diameter >99.95% purity W rod supplied by Eagle Alloys Corporation using wire EDM, after which the surface was partially ground using 600-grit $SiO_2$ paper. The oxygen content of the plate reported by the manufacturer was 30 ppm. A Keyence VK-X100 3D laser scanning microscope was used for a posteriori top surface examination of the cracks. 10 two mm long lines were scanned using each of the five parameter combinations in Table 1.

## 3. Results & Discussion

Except for one track in which a longitudinal crack appeared (outside of the camera field of view), all cracks were transverse. This allowed quantification of the time delay in milliseconds (Crack delay [ms] in Table 1) between the passage of the tail end of the melt pool and the appearance of a crack, which could also be converted to a distance behind the melt pool (Crack delay [µm] in Table 1). Since many videos showed multiple cracks, the distance between cracks could also be extracted (Crack spacing [µm] in Table 1). A metric containing similar information was derived from a posteriori examination of the scan tracks by dividing the total track length by the total number of cracks (Distance per crack [µm] in Table 1). This last metric, however, does not take end effects (start and end of a track) into account.

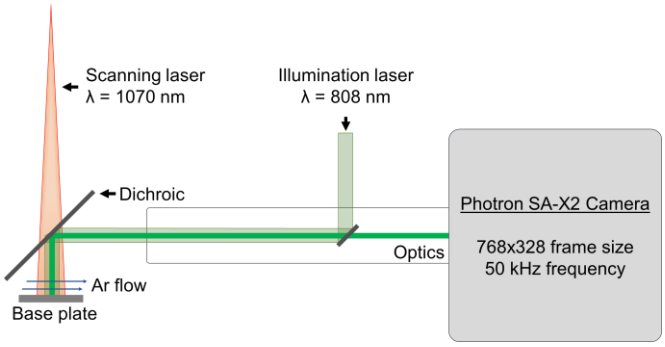


Fig. 1. Schematic of the experimental setup with indication of the major components.

Table 1. Overview of the different parameter sets, and their metrics extracted via in-situ monitoring.

| P [W] | v [mm/s] | Melt width [µm] | Crack delay [ms] | Crack delay [µm] | Crack spacing [µm] | Distance per crack [µm] |
|---|---|---|---|---|---|---|
| 300 | 50 | 100 ± 1 | 14 ± 10 | 692 ± 478 | 216 ± 120 | 421 |
| 300 | 100 | 96 ± 2 | 6 ± 2 | 581 ± 212 | 237 ± 158 | 407 |
| 300 | 300 | 89 ± 2 | 1.7 ± 1.3 | 496 ± 391 | 261 ± 84 | 357 |
| 450 | 100 | 141 ± 2 | 9 ± 2 | 884 ± 232 | 333 ± 135 | 571 |
| 450 | 300 | 126 ± 2 | 2.4 ± 0.7 | 726 ± 222 | 357 ± 135 | 541 |

The large spread of the results in Table 1 reflects the stochastic nature of the microcracking. Local variations in grain boundary area, misorientation and possible defects may lead to earlier formation of a crack or inhibit a crack to form in a specific location. In some tracks, cracks would appear simultaneously several hundred µm apart, whereas other cracks propagated across the track in steps. Some cracks propagated away from the track far into the plate. In all videos, a heat wave in front of the laser caused surface cracks to appear on the base plate. The cause and relevance of these phenomena are not under investigation here but are the subject of future work.

Due to the anisotropic thermal shrinkage of differently oriented grains, the solidification structure forms a topology on the surface of the track and reveals an equiaxed microstructure with a slight elongation in the longitudinal direction of the track, as shown in Figure 2. For higher scan speeds, the surface ripples left by the melt pool obscure the solidification structure. The cracks are intergranular in nature, highlighting that the grain boundaries are the biggest weakness of tungsten at low temperature.

Figure 3 shows four camera frames in which the laser scans from left to right at $v$ = 100 mm/s, using $P$ = 300 W.

The melt pool is visible in (a) and (b). In (b)-(d), the frame just after the appearance of a crack is shown, and the crack location is highlighted in red. Most cracks appeared instantaneously, and it was not possible to determine the crack propagation speed using a 50 kHz frame rate.

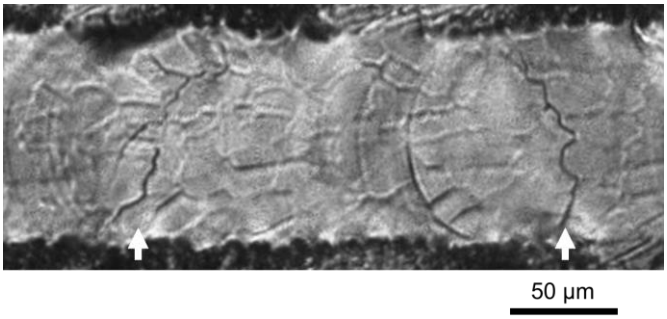


Fig. 2. Track topology for $P$ = 300 W and $v$ = 50 mm/s, showing equiaxed grains elongated in the scan direction, and two intergranular cracks indicated by the arrows. The laser moved from left to right.

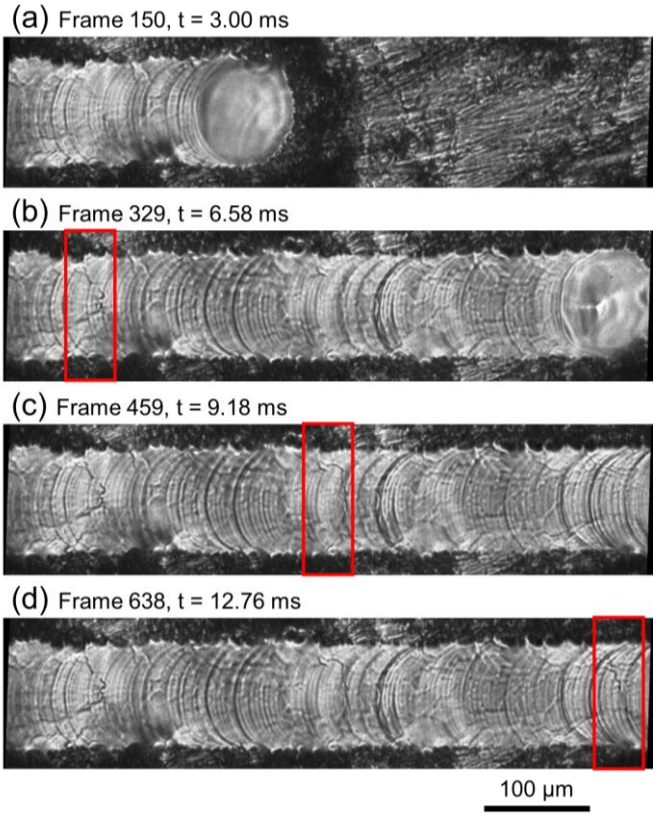


Fig. 3. Example of the in-situ monitoring results for $P$ = 300 W and $v$ = 100 mm/s, highlighting the location of three cracks in red. The first frame after each crack appearance ((b): Crack 1, (c): Crack 2, (d): Crack 3) is shown.

As expected, the melt pool width decreases with increasing speed, and is larger for higher powers, shown in Figure 4(a). An increase in scan speed reduces the time delay between passage of the melt and crack initiation (Figure 4(b)). Converting the time delay to the distance behind the melt pool reduces this dependence on the scan speed, and in Figure 4(c) the slight downward trend for increasing scan speeds falls within the error bars. A more obvious effect is that the higher power parameter sets have a longer delay (in terms of distance) after passage of the melt pool before a crack is formed, and the distance between cracks also seems to be larger (Figure 4 (d)). Indicated by hollow markers in Figure 4(d), this trend is also observed when dividing the total scan length of all tracks for a certain parameter combination by the total number of cracks. Due to the large spread on the results, no conclusions can be drawn about the influence of the scan speed.

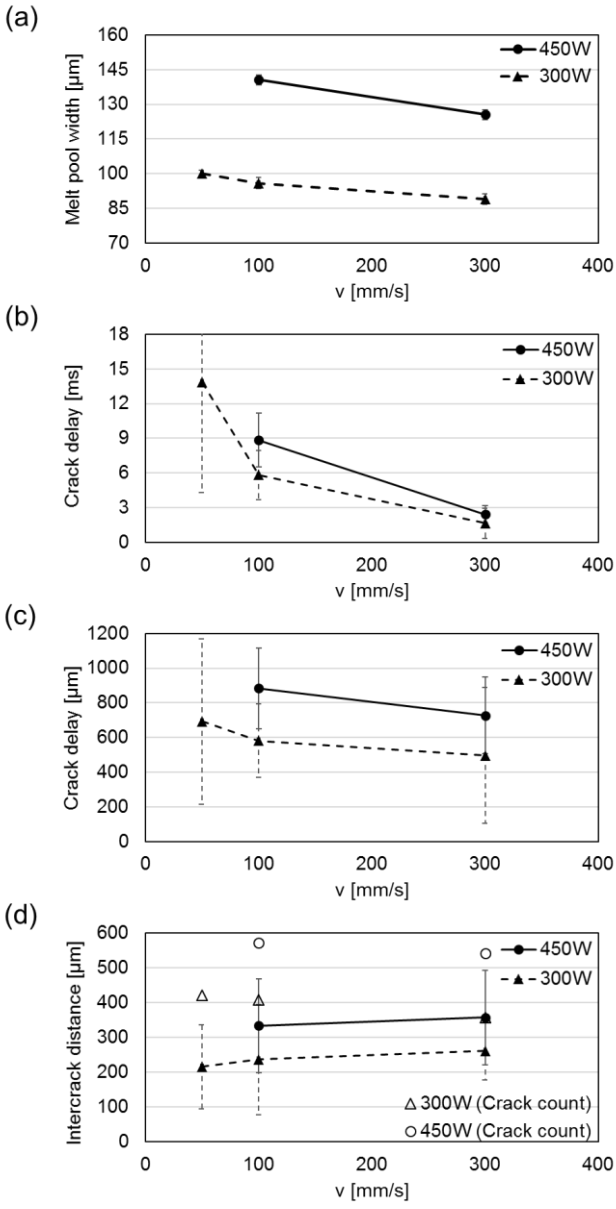


Fig. 4. (a) Melt pool width; (b) Crack spacing; (c) Crack delay after passage of the melt in milliseconds and (d) in micrometers. In (b), the hollow markers are data points for which the total length of track was divided by the total number of cracks.

The most probable cause for this correlation between the crack delay and power is that a higher power leads to an increase in overall temperature, and that the solidified track stays warmer for longer. The current hypothesis in literature is that the ductile-to-brittle transition causes of the microcracks in SLM of W, which occurs at a given temperature [2]. A higher heat input from the laser therefore means that the material must cool longer to reach this temperature. It is

unclear why using a slower scan speed, which should have a similar effect, did not lead to similar results. Furthermore, the reduction in the number of cracks (Figure 4(d)), is likely caused by the lower thermal gradients when using a high laser power.

The time delay for cracks to appear is on the order of milliseconds (see Figure 4(b)). In that timespan, the laser travels a couple hundred microns for $v$ = 100 mm/s. It is therefore unlikely that an adjacent scan track has an influence on the primary crack formation in the original track. It does, however, reheat the area and impose transverse shrinkage strains and may therefore cause additional, possibly longitudinal, cracks to form.

In future work, the high-speed video monitoring will be combined with thermal models to estimate the temperature profile behind the melt pool, specifically in the area where cracks appear, and to elucidate the different response of microcracks to an increased laser power compared to a lower scan speed. Multiple tracks will be deposited adjacent to each other to determine the influence of reheating and imposing a transversal strain component on both the existing cracks in the first track, as well as the appearance of new cracks.

## 4. Conclusion

Using in-situ high speed monitoring, the exact moment of crack initiation during Selective Laser Melting of W was characterized. Through analysis of five different parameter sets, it was found that a high laser power reduces the number of cracks through a higher crack spacing and increases the time it takes for a crack to form after passage of the melt pool. Analysis of the influence of conventional process parameters on microcracking in SLM may lead to preferential scanning strategies to be used for W.

## Acknowledgements

The author would like to thank Gabe Guss for assisting with the alignment of the experimental setup. This work was performed under the auspices of the U.S. Department of Energy by Lawrence Livermore National Laboratory under Contract No. DE-AC52-07NA27344. This work was funded by the Laboratory Directed Research and Development Program at LLNL under project tracking code 18-ERD-057 and 18-SI-003.

## References

[1] T. Hirai and G. Pintsuk, “Thermo-mechanical calculations on operation temperature limits of tungsten as plasma facing material,” *Fusion Eng. Des.*, vol. 82, no. 4, pp. 389–393, Jun. 2007.

[2] A. Iveković *et al.*, “Selective laser melting of tungsten and tungsten alloys,” *Int. J. Refract. Met. Hard Mater.*, vol. 72, pp. 27–32, Apr. 2018.

[3] B. Vrancken, R. Wauthle, J.-P. Kruth, and J. Van Humbeeck, “Study of the influence of material properties on residual stress in selective laser melting,” in *Proceedings of the Solid Freeform Fabrication Symposium*, Austin, TX, 2013, pp. 393–407.

[4] X. Zhou, X. Liu, D. Zhang, Z. Shen, and W. Liu, “Balling phenomena in selective laser melted tungsten,” *J. Mater. Process. Technol.*, vol. 222, pp. 33–42, Aug. 2015.

[5] D. Wang, C. Yu, X. Zhou, J. Ma, W. Liu, and Z. Shen, “Dense Pure Tungsten Fabricated by Selective Laser Melting,” *Appl. Sci.*, vol. 7, no. 4, p. 430, Apr. 2017.

[6] V. Krsjak, S. H. Wei, S. Antusch, and Y. Dai, “Mechanical properties of tungsten in the transition temperature range,” *J. Nucl. Mater.*, vol. 450, no. 1, pp. 81–87, Jul. 2014.

[7] P. Gumbsch, “Brittle fracture and the brittle-to-ductile transition of tungsten,” *J. Nucl. Mater.*, vol. 323, no. 2, pp. 304–312, Dec. 2003.

[8] E. Gaganidze, D. Rupp, and J. Aktaa, “Fracture behaviour of polycrystalline tungsten,” *J. Nucl. Mater.*, vol. 446, no. 1, pp. 240–245, Mar. 2014.

[9] M. Battabyal, R. Schäublin, P. Spätig, and N. Baluc, “W–2wt.%Y2O3 composite: Microstructure and mechanical properties,” *Mater. Sci. Eng. A*, vol. 538, pp. 53–57, Mar. 2012.

[10] S. Antusch *et al.*, “Mechanical and microstructural investigations of tungsten and doped tungsten materials produced via powder injection molding,” *Nucl. Mater. Energy*, vol. 3–4, pp. 22–31, Jul. 2015.

[11] J. R. Stephens, “Effects of Interstitial Impurities on the Low-Temperature Tensile Properties of Tungsten,” Lewis Research Center, National Aeronautics and Space Administration Cleveland OH, NASA-TN-D-2287, Jun. 1964.

[12] B. Huang *et al.*, “Effect of potassium doping on the thermal shock behavior of tungsten,” *Int. J. Refract. Met. Hard Mater.*, vol. 51, pp. 19–24, Jul. 2015.

[13] R. I. Jaffee and G. T. Hahn, “Structural Considerations in Developing Refractory Metal Alloys,” p. 37, Jan. 1963.

[14] B. Gludovatz, S. Wurster, A. Hoffmann, and R. Pippan, “Fracture toughness of polycrystalline tungsten alloys,” *Int. J. Refract. Met. Hard Mater.*, vol. 28, no. 6, pp. 674–678, Nov. 2010.

[15] M. V. Aguirre, A. Martín, J. Y. Pastor, J. LLorca, M. A. Monge, and R. Pareja, “Mechanical properties of tungsten alloys with Y2O3 and titanium additions,” *J. Nucl. Mater.*, vol. 417, no. 1, pp. 516–519, Oct. 2011.

[16] T. Hirai, G. Pintsuk, J. Linke, and M. Batilliot, “Cracking failure study of ITER-reference tungsten grade under single pulse thermal shock loads at elevated temperatures,” *J. Nucl. Mater.*, vol. 390–391, pp. 751–754, Jun. 2009.

[17] S. Ly, A. M. Rubenchik, S. A. Khairallah, G. Guss, and M. J. Matthews, “Metal vapor micro-jet controls material redistribution in laser powder bed fusion additive manufacturing,” *Sci. Rep.*, vol. 7, no. 1, p. 4085, Jun. 2017.